Journal of Power Sources 195 (2010) 4583–4592

Contents lists available at ScienceDirect

Journal of Power Sources

journal homepage: www.elsevier.com/locate/jpowsour

Tolerance tests of H_2S-laden biogas fuel on solid oxide fuel cells

Chunchuan Xu[a], John W. Zondlo[a,*], Mingyang Gong[b], F. Elizalde-Blancas[b], Xingbo Liu[b], I.B. Celik[b]

[a] Department of Chemical Engineering, West Virginia University, Morgantown, WV 26506, USA
[b] Department of Mechanical & Aerospace Engineering, West Virginia University, Morgantown, WV 26506, USA

ARTICLE INFO

Article history:
Received 22 December 2009
Received in revised form 24 February 2010
Accepted 25 February 2010
Available online 3 March 2010

Keywords:
SOFC
Ni–YSZ anode
Biogas
CH_4 reforming
Ni–CeO_2 coating
H_2S contaminant

ABSTRACT

Biogas is a variable mixture of methane, carbon dioxide and other gases. It is a renewable resource which comes from numerous sources of plant and animal matter. Ni–YSZ anode-supported solid oxide fuel cell (SOFC) can directly use clean synthesized biogas as fuel. However, trace impurities, such as H_2S, Cl_2 and F_2 in real biogas can cause degradation in cell performance. In this research, both uncoated and coated Ni–YSZ anode-supported cells were exposed to three different compositions of synthesized biogases (syn-biogas) with 20 ppm H_2S under a constant current load at 750–850 °C and their performance was evaluated periodically using standard electrochemical methods. Postmortem analysis of the SOFC anode was performed using X-ray diffraction (XRD), scanning electron microscopy (SEM) and X-ray photoelectron spectroscopy (XPS). The results show that H_2S causes severe electrochemical degradation of the cell when operating on biogas, leading to both complete electrochemical and mechanical failure. The Ni–CeO_2 coated cell showed excellent stability during CH_4 reforming and some tolerance to H_2S contamination.

1. Introduction

Biogas is a potential source fuel for the SOFC by direct internal reforming (DIR) at the SOFC anode. It is a cheap and renewable fuel available from many sources, such as landfill gas, biomass, sewage, municipal waste, green waste and energy crops [1]. The composition of biogas is a complex and variable mixture of CH_4 and CO_2 while containing a few percent of N_2, H_2, O_2 and trace contaminants such as H_2S, Cl_2 and F_2. Furthermore the Ni–YSZ anode with its "in situ" nickel catalyst and high operation temperature makes DIR of biogas possible. DIR offers not only excellent heat transfer and simple, cost-effective design for the SOFC system, but also gives great system efficiency for electrical power generation [2]. Although carbon deposition or carbon build-up on the nickel in the anode (coking) is still a barrier to DIR, coke-free reforming can be obtained at a small sacrifice in efficiency. Lin et al. reported that the Ni–YSZ anode-supported SOFC can be operated without coking over a wide range of current density by fueling humidified (3% H_2O) CH_4 at temperatures $\leq$700 °C, or under high current density load ($J \geq 1.8\,A\,cm^{-2}$) at temperature $\geq$800 °C [3]. Steam reforming with high steam to CH_4 ratio (S/C > 1) and doping additional catalysts in the Ni–YSZ anode, such as Mo, Pt, Ru, Au, and La, have been reported in the literature [4–8]. A major drawback of steam reforming is the intensive energy requirement due to the high endothermic reforming reactions which create thermal gradients on the anode and can lead to cell or current collector cracking or damage. The application of partial oxidation of CH_4 as an alternative route for reforming biogas has been suggested as a means of avoiding carbon coking and cell cracking [9,10]. However, most biogas contains several sulfur compounds as contaminants at different concentration levels and these are converted into H_2S at SOFC operation temperatures. The effects of H_2S contamination on the Ni–YSZ anode of SOFC in H_2 and syngas fuels have been reported in many research papers. The two primary mechanisms to cause Ni–YSZ anode degradation are physical adsorption of sulfur that blocks the hydrogen reaction sites and chemical reaction that forms nickel sulfide leading to the complete loss of Ni catalysis [11]. Sulfur adsorption is generally considered as the major cause for anode degradation at low H_2S concentration in the fuel (typically below 20 ppm). For SOFCs operating with higher concentrations of H_2S, formation of nickel sulfide on the anode surface appeared to account for the performance loss [12]. However, the degradation of cell performance can be at least partially recovered after cutting off the H_2S flow in the H_2 or syngas fuel. More severe cell deterioration can occur in DIR of CH_4 with H_2S impurity when using the SOFC with a Ni–YSZ anode [13], but experimental data on H_2S contamination of hydrocarbon fuel for DIR on the Ni–YSZ anode SOFC has never been reported.

This paper reports that the Ni–YSZ anode-supported SOFC can be operated stably and long term on synthesized biogas at 850 °C. However, the cell was devastated in a few hours after co-feeding an additional 20 ppm of H_2S. The addition of ceria into the impregnated Ni–YSZ anode showed good CH_4 reforming performance and high resistance to carbon deposition [14–19]. Moreover, ceria is widely used as an H_2S-removal catalyst [20,21]. To resist H_2S

* Corresponding author. Tel.: +1 304 293 9366; fax: +1 304 293 4139.
E-mail address: John.Zondlo@mail.wvu.edu (J.W. Zondlo).

0378-7753/$ – see front matter © 2010 Elsevier B.V. All rights reserved.
doi:10.1016/j.jpowsour.2010.02.078

attack and improve the internal CH_4 reforming, a Ni–CeO_2 coated anode-supported SOFC was tested for use in DIR of CH_4 with H_2S contamination. Tests with the treated anode showed good overall cell performance along with some tolerance to H_2S attack.

2. Experimental methods

2.1. Experiment setup

For this study, commercial Ni–YSZ anode-supported SOFCs produced by Materials and Systems Research Inc., in Salt Lake City, UT, USA, were used in the experiment. The cell composition and the current collection contact configuration were described in a previous paper [22]. The button cell assembly was mounted in a furnace operated at 850 °C which affords reasonable performance for all different fuel compositions in the test series. A thermocouple was set located 5 mm away from the center of the cell cathode to monitor the change of cell temperature. Alicat Scientific mass flow controllers were used to control the fuel and air stream flow rates and compositions. The flow rates of CH_4, H_2O, CO_2, H_2S (1000 ppm H_2S in N_2) and air were each controlled separately. A temperature-controlled humidifier was used to adjust the H_2O concentration of the simulated biogas provided to the anode. The composition mole ratio of $CH_4/CO_2 = 1$ was used for internal dry reforming (IDR). The composition mole ratio of $CH_4/CO_2 = 1.6$ and 1.5 was used for internal steam reforming (ISR) and internal air with steam reforming (IASR) respectively. After adding steam and air with steam to the fuel, the total flow rate was held at 200 sccm (standard cubic centimeters per minute) and the air-flow rate to the cathode was kept constant at 300 sccm. The anode fuel transfer lines were heat-traced to prevent water condensation between the humidifier and furnace. The CH_4 and air in the fuel stream flowed through the temperature controllable humidifier and picked up the H_2O vapor. CO_2 and H_2S were injected down-stream of the anode humidifier close to the furnace to ensure all trace species injected into the stream reached the anode of the SOFC. To increase the cell tolerance toward coking, cracking and H_2S, a Ni–CeO_2 coating was painted on top of the cell anode surface after the current collection meshes had been attached. The Ni–CeO_2 coated cell cross-sectional profile is shown in Fig. 1. The Ni–CeO_2 coating paste is made of 90% Ni and 10% CeO_2 (by weight) powder mixed with terpineol vehicle by sonic stirring for 2 h before printing on the cell anode and the anode contacts. Then the cell coated with the Ni–CeO_2 paste is heated to 800 °C for 2 h in air at atmospheric pressure.

2.2. Electrochemical testing of the SOFC performance

The button SOFC was heated from room temperature to 800 °C at a rate of 5 °C min^{-1}. After the cell was completely reduced in H_2, the open circuit voltage (OCV) was 1.072 V with 97% H_2, 3% H_2O on the anode side and air (21% O_2) on the cathode side. This is a bit lower than the theoretical OCV presumably because of slight leakage around the cell seals and possibly through the electrolyte. Then, 0.25 A cm^{-2} direct current (DC) was loaded for a current treatment overnight (10 h). The constant DC current load was supplied by a solid-state load cell (TDI Transistor Device SD-1103). After loading the SOFC at a constant current density of 0.5 A cm^{-2} for another 24 h, the cell voltage stabilized at 0.785 V. Then CH_4 internal reforming was commenced by flowing three different syn-biogas compositions on three different SOFCs at a prescribed temperature. The performance of the different cells was less than ±5% under similar test conditions.

The electrochemical impedance spectra were collected using a Solartron SI-1287 electrochemical interface and an SI-1260 frequency response analyzer with an AC amplitude of 20 mV at frequencies ranging from 100 kHz to 0.1 Hz. Direct internal syn-biogas reforming experiments were carried out under 1 atm pressure at the following different reforming conditions.

(1) IDR at 750 °C, 800 °C and 850 °C.
(2) ISR without and with the Ni–CeO_2 coating at 850 °C.
(3) IASR without and with the Ni–CeO_2 coating at 850 °C.

2.3. Chemical, structural and thermodynamic analysis

The microstructure and chemical composition of the cell anode were examined with a Hitachi S-4700 SEM/EDS. To determine the composition of the anode, an XRD (Panalytical X'Pert Pro PM-3040) with a Cu K-alpha radiation source (1.54060 Å), and an XPS (PHI 5000 VerasProbe XPS Microprobe) with a monochromatic Al K-alpha radiation source (8.34118 Å) were employed. Thermodynamic equilibrium calculations were carried out to predict H_2, CO, CO_2 and H_2O concentrations under biogas reforming conditions by using the FACTSAGE 5.4 software package.

3. Results

3.1. IDR at 750 °C, 800 °C and 850 °C

After feeding 60 sccm CH_4 and 60 sccm CO_2 ($CH_4/CO_2 = 1$) as the fuel in place of H_2, the temperature dependent IDR polarization data were taken (Fig. 2). The open circuit voltage (OCV) at the IDR condition increased with cell reforming temperature. At 750 °C, 800 °C and 850 °C, the cell OCV was 0.994 V, 1.025 V and 1.049 V, along with the maximum power density of 0.313 W cm^{-2}, 0.411 W cm^{-2} and 0.547 W cm^{-2} respectively. Both the equilibrium calculations and experiment suggest that the IDR at 850 °C gives high H_2 and CO conversion efficiency and high power density under the same loading when compared to that at 800 °C and 750 °C. So the subsequent long-term test was carried out at 850 °C in the

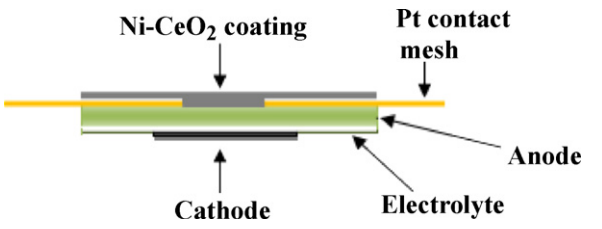

Fig. 1. The Ni–CeO_2 coated cell cross-sectional profile. The Ni–CeO_2 layer is about 100 μm and 350 μm in the ISR and IASR cases respectively.

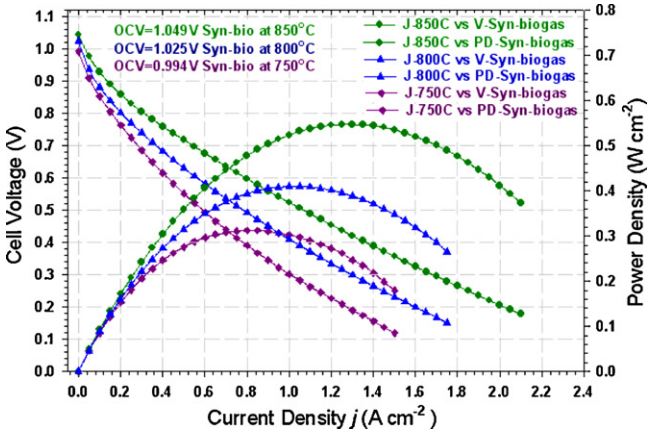

Fig. 2. The polarization and power density curves under internal dry reforming of 120 sccm syn-biogas with CH_4:CO_2 = 1:1 (mole ratio) in the SOFC system at T = 750 °C, 800 °C and 850 °C.

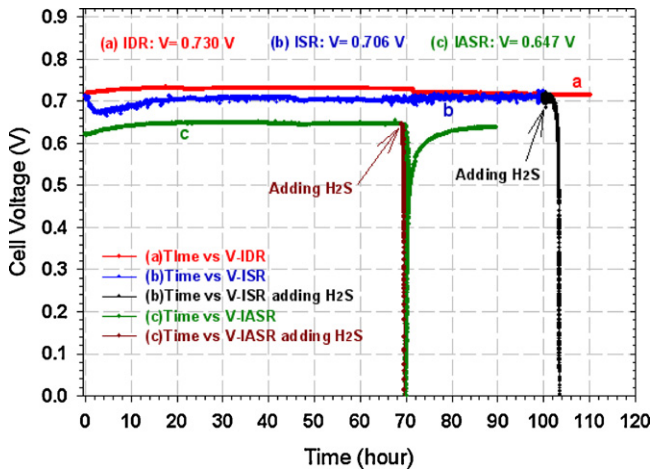

Fig. 3. The time versus cell voltage plots in three internal reforming syn-biogas conditions. (a) Internal dry reforming (IDR). (b) Internal steam reforming (ISR) syn-biogas and adding 20 ppm H_2S for 3 h. (c) Internal air with steam reforming (IASR) and adding 20 ppm H_2S for 0.7 h.

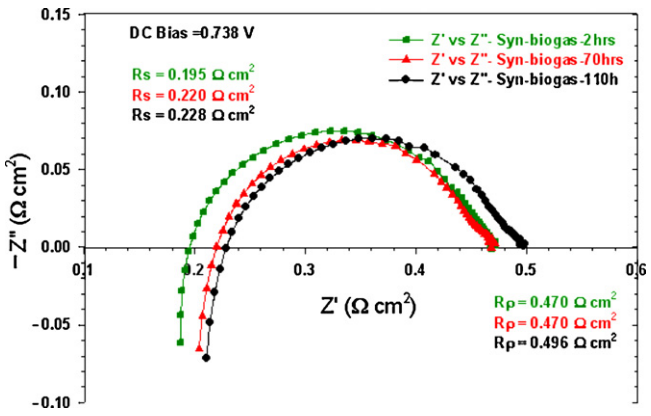

Fig. 4. The cell impedance spectra taken at 2 h, 70 h and 110 h for IDR reforming.

remaining investigations. At 850 °C, the cell voltage stabilized at 0.720 V under a loaded current density of 0.5 A cm^{-2} for 72 h. After taking the electrochemical impedance spectrum (EIS), the cell voltage slightly dropped to 0.710 V and continually ran at this level for another 40 h (see line (a) in Fig. 3). The cell was then cooled down to room temperature by purging the anode with 20% H_2 with 80% N_2. The EIS data showed that both the cell series resistance and the total polarization resistance increased with reforming time (Fig. 4). The cell anode surface was inspected and revealed severe coking on the cell anode. A deposit of carbon about 0.10–0.15 g covered nearly 4 cm^2 of the anode (Fig. 5(a)). The Pt contact meshes on the anode surface were broken and lost good contact. The exposed anode center area between the two Pt meshes showed carbon deposited in the pore structure of the anode surface (Fig. 5(b)). Because the deposition of carbon was significant, the H_2S contaminant test was not carried out for the IDR case. But studying the IDR case provided a basic guideline to further study of the ISR and IASR of CH_4.

3.2. ISR without and with the Ni–CeO_2 coating at 850 °C

After 60 sccm CH_4 passed through the humidification tank thereby adding steam (H_2O) to the biogas fuel, the initial composition of syn-biogas fuel was 32% CH_4, 48% H_2O and 20% CO_2 with a total flow rate of 200 sccm. This fuel gas gave the uncoated cell OCV of 0.925 V at 850 °C. After 0.5 A cm^{-2} loading for about 15 h, the voltage stabilized at 0.708 V and the EIS data were subsequently taken periodically. As seen in Fig. 6, the cell series resistance increased from 0.184 Ω cm^2 to 0.253 Ω cm^2, but the total resistance stayed nearly constant around 0.440 Ω cm^2. After running for about 100 h, the cell was cooled down to room temperature and the anode surface was examined. The current collection contacts partially cracked and lost conduction contact to the anode which explained the slight increase of the series resistance. There was some carbon deposited only on the contact surface of the anode side but not nearly as much as in the IDR case. The contacts were repaired and the cell was reloaded and run at the same conditions stably for 2 h, whereupon 20 ppm H_2S was injected down-stream of the humidifier into the syn-biogas fuel. The cell voltage was constant at 0.708 V for about 1.5 h, then the voltage quickly and catastrophically dropped to a negative value in about 3 h (see line (b) in Fig. 3). The cell was cooled to room temperature while purging with N_2. Upon inspection, it was found that the cell electrolyte layer was cracked along the cathode edge and fully separated from the anode with the cathode and Pt contact mesh. The green patterns are displayed on the opened anode/electrolyte interface of the cell center, indication oxidation of the nickel (Fig. 7). A similar mechanical failure occurred in the IASR case.

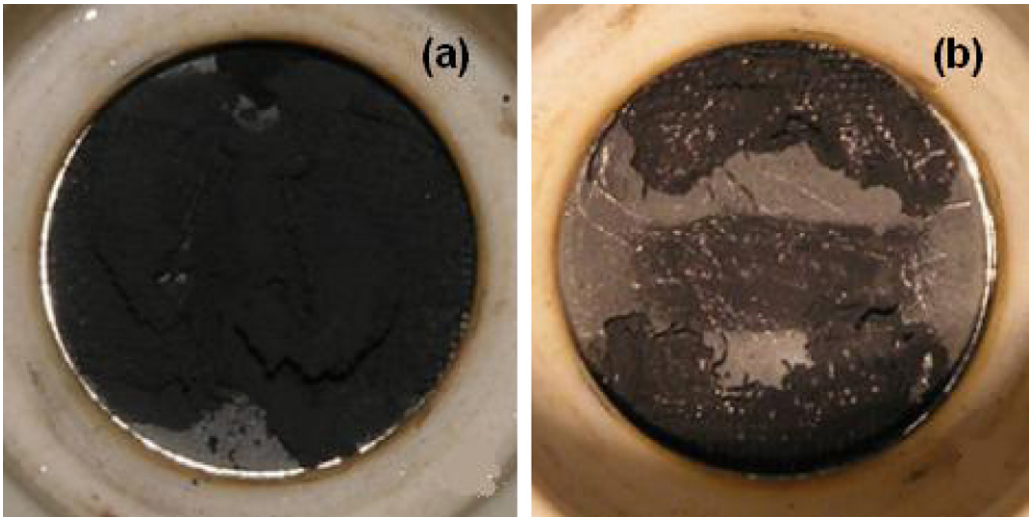

Fig. 5. (a) A significant deposition of carbon on the cell anode surface after 110 h IDR reforming. (b) After removing the deposited carbon powder, the broken Pt connecting meshes were displayed. The exposed cell region is about 2 cm diameter.

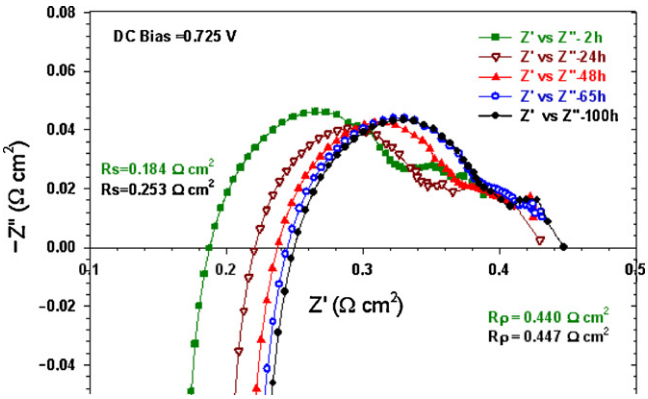

Fig. 6. The cell impedance data taken at 2 h, 24 h, 48 h, 65 h and 100 h before adding 20 ppm H_2S in ISR reforming.

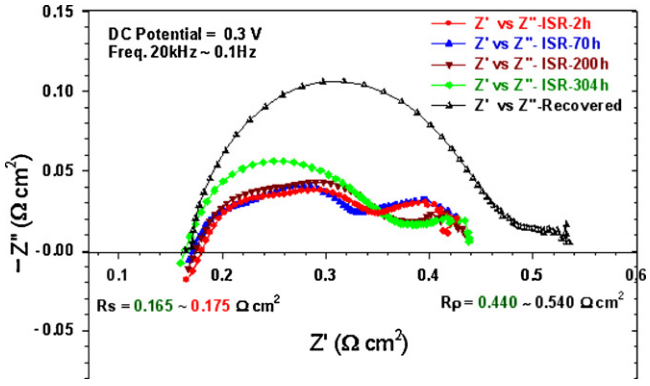

Fig. 8. The changes of the Ni–CeO_2 coated cell impedance spectra before adding 20 ppm H_2S and after recovery of one H_2S contamination cycle in ISR.

Significant coking and contact cracking were observed in the uncoated cell anode of the ISR case. Furthermore, 20 ppm H_2S contamination in the ISR fuel system leads to irreversible cell failure and complete loss of performance in a few hours. On the other hand, a Ni–CeO_2 coated cell may provide an H_2S barrier layer and an additional reforming layer which could enhance the CH_4 reforming sites and surface area and minimize coking and cracking. Further the relatively sparse structure of the Ni–CeO_2 layer can relieve the thermal expansion stress resulting from the endothermic reforming reactions. Thus a cell was coated with a layer of approximately 100 μm Ni–CeO_2 on the anode. Comparing the performance of the coated cell with that of the uncoated cell, the Ni–CeO_2 coated cell had almost equivalent electrochemical performance. After the coated cell was running for about 304 h under ISR conditions at 850 °C at a constant 0.5 A cm^{-2} load, the cell voltage gradually stabilized at 0.732 V. The impedance spectra were taken at 2 h, 70 h, 200 h, and 304 h as seen in Fig. 8. The series and polarization resistances did not increase significantly before adding the H_2S contamination. The 20 ppm H_2S was then added to the fuel stream and the cell performance plots of the Ni–CeO_2 coated cell are shown in Fig. 9. The cell operated unchanged in the presence of the H_2S for about 2 h after which the cell voltage dropped to 0 V in an additional 2 h. Recalling that the uncoated cell was broken and the cell performance was not reversible (Fig. 3(b)), the voltage of the coated cell could be recovered to 0.650 V after stopping the H_2S flow for 24 h. Moreover the coated cell anode surface did not show significant coking and the current contacts were not cracked. This suggests that the Ni–CeO_2 coating can increase coking resistance and enhance tolerance of H_2S poisoning as seen in this preliminary test.

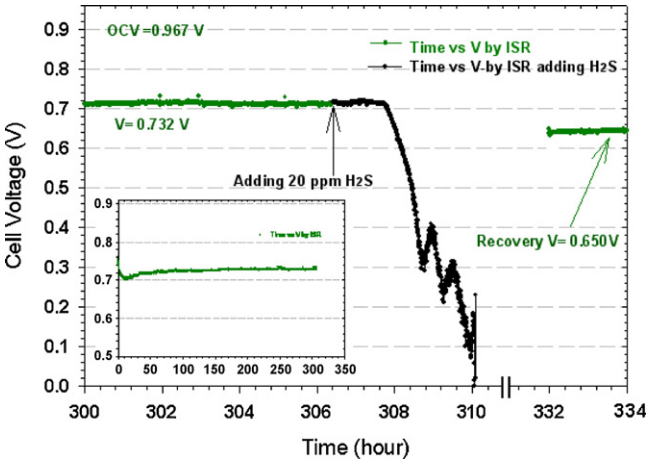

Fig. 9. The cell voltage loss of the Ni–CeO_2 coated cell after adding 20 ppm H_2S impurity for 4 h. But it can be recovered to 0.650 V after cutting off H_2S flow for 24 h.

The endothermic reforming reactions can be observed by the fact that the cell temperature dropped below the furnace control temperature during biogas reforming in both the coated and uncoated ISR cases. The cell temperature under 0.5 A cm^{-2} load was around 844 °C which is lower than the furnace control temperature

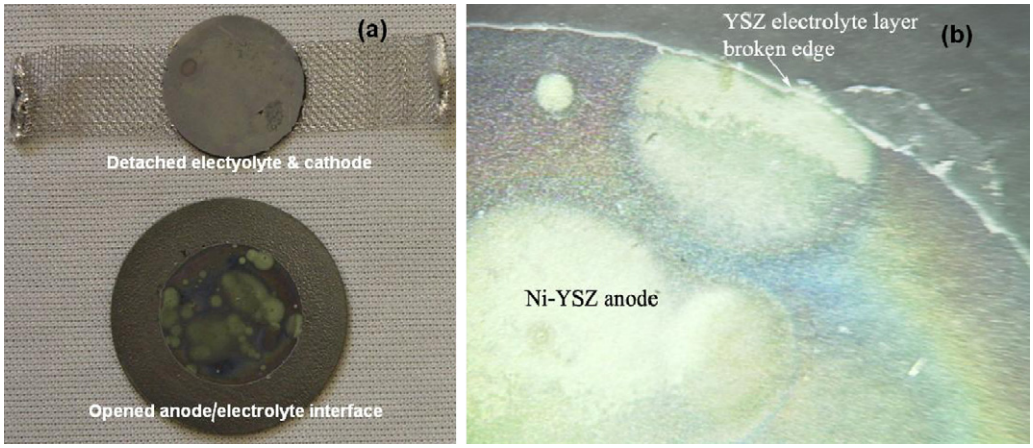

Fig. 7. (a) The postmortem cell cathode side images after poisoning by 20 ppm H_2S impurity in ISR case. The cell cathode and electrolyte along with the current collection Pt mesh was detached from the cell. A green pattern of the anode/electrolyte interface is displayed on the cell anode interface center. (b) The detailed image of the broken electrolyte/anode interface surface. The cell anode diameter is 2.54 cm. (For interpretation of the references to color in this figure legend, the reader is referred to the web version of the article.)

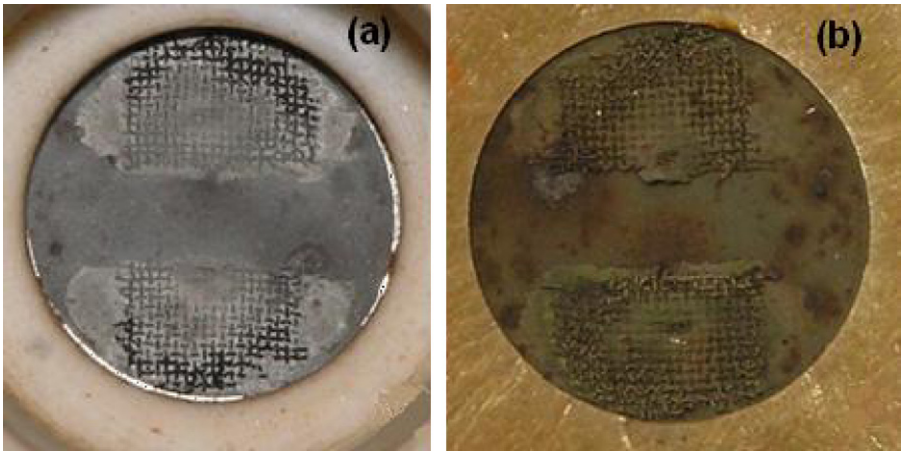

Fig. 10. (a) The cell anode image after IASR for 50 h. There is slight coking on the Pt current connection meshes. (b) The cell anode image after two cycles adding 20 ppm H_2S, the cell lost all its performance. The anode surface was oxidized to green. The exposed cell region is about 2 cm diameter. (For interpretation of the references to color in this figure legend, the reader is referred to the web version of the article.)

of 850 °C. Because the thermocouple was 5 mm away from the cell cathode, the actual cell temperature may be even lower than 844 °C.

3.3. IASR without and with the Ni–CeO_2 coating at 850 °C

By injecting 60 sccm CH_4 mixed with 60 sccm air into the humidifier water tank, the mixed gas brings steam into the syn-biogas fuel mixture. The initial composition of syn-biogas is 30% CH_4, 30% air (6.3% O_2), 20% H_2O and 20% CO_2 with a total flow rate of 207 sccm. The uncoated cell OCV of 0.962 V was found at 850 °C for the IASR case. Under 0.5 A cm^{-2} load for about 10 h, the voltage stabilized at 0.647 V. After the cell operated for about 50 h stably, the cell was cooled down to room temperature and taken out from the furnace to check the anode surface. There was no visible coking on the cell anode center and no cracking of the contacts. Only slight carbon deposits were observed on the contact Pt meshes areas (Fig. 10(a)). After observing the coking, the cell was reloaded and operated under the same IASR conditions for another 20 h without any loss of the cell performance. At this point, 20 ppm H_2S was injected in the syn-biogas fuel. The cell voltage degraded to zero in less than 40 min. After the cell voltage dropped to zero, the H_2S flow was cut off whereupon the cell voltage slowly recovered to 0.638 V (recovery 98.7%) in about 20 h (see line (c) in Fig. 3). The EIS data were taken before adding the 20 ppm H_2S and after recovery in the first cycle (Fig. 11). The increasing series resistance prior to H_2S addition implies that some coking and contact cracking may still have occurred. When the recovered cell voltage was stabilized at 0.638 V, 20 ppm H_2S was again fed in the fuel stream for a second cycle. The cell voltage started to drop immediately and fell to −0.4 V after 50 min. The cell voltage could not be recovered after the H_2S flow was cut off in the second contamination cycle. The cell OCV was unstable and fluctuated between 0.910 V and 0.780 V. The postmortem cell anode was green in color (Fig. 10(b)) and the cell electrolyte and cathode along with its Pt mesh were separated from the anode base (this same mechanical failure also occured in the case of the ISR in the uncoated cell (Fig. 7)). The postmortem cell was subjected to chemical and structural analysis, described below.

A Ni–CeO_2 coated cell was also tested in the IASR reforming case as well. The Ni–CeO_2 coating layer was about 350 μm on the anode surface. The coated cell voltage under IASR conditions was about 0.660 V for a current density of 0.5 A cm^{-2} at 850 °C. The series and polarization resistances remained almost constant at 0.302 Ω cm^2 and 0.580 Ω cm^2 in 70 h respectively (Fig. 12). After about 70 h of stable operation in the IASR condition, 20 ppm H_2S was added to the fuel for the "first cycle." By resetting the time axis, comparison plots are shown in Fig. 13. In 40 min, the coated cell lost about 128 mV at a constant current of 0.5 A cm^{-2} whereas the uncoated cell lost all its performance in the same time period. Both cells were recovered to 0.631 V (recovery 95.6%) for the coated cell and 0.642 V (recovery 99.2%) for the uncoated cell. During the second cycle of injecting H_2S for 50 min, the uncoated cell was completely damaged, but the coated cell could again be recovered to 0.612 V (recovery 96%). It

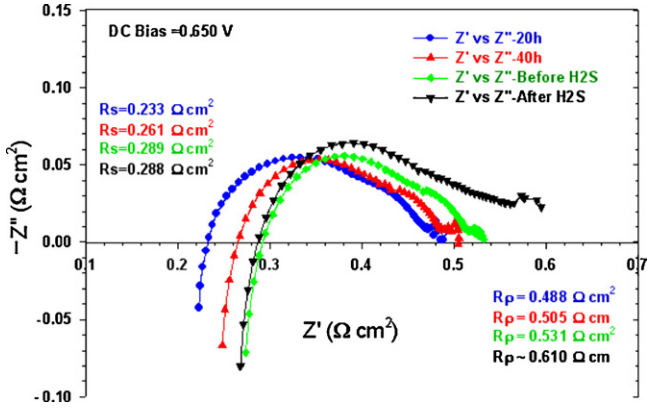

Fig. 11. The cell impedance spectra before adding 20 ppm H_2S and after recovery of the first cycle in IASR.

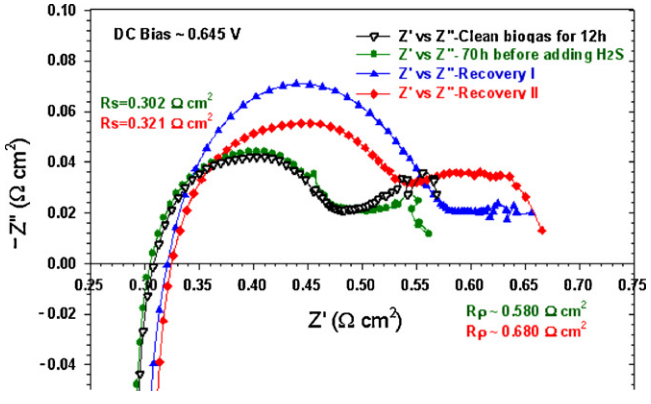

Fig. 12. Comparison of the voltage loss between the Ni–CeO_2 coated cell and uncoated cell in IASR after adding 20 ppm H_2S impurity for 40 min in the first cycle (the time axis was adjusted for comparison).

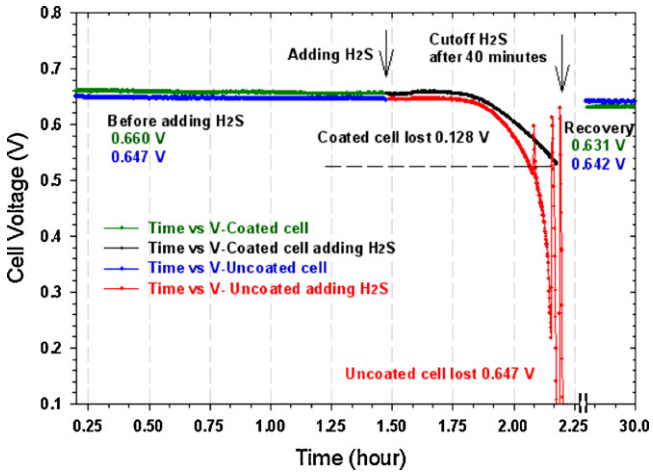

Fig. 13. Comparison of the loss of voltage between the Ni–CeO_2 coated cell and uncoated cell after adding 20 ppm H_2S impurity for 50 min in the second cycle (the time axis was adjusted for comparison).

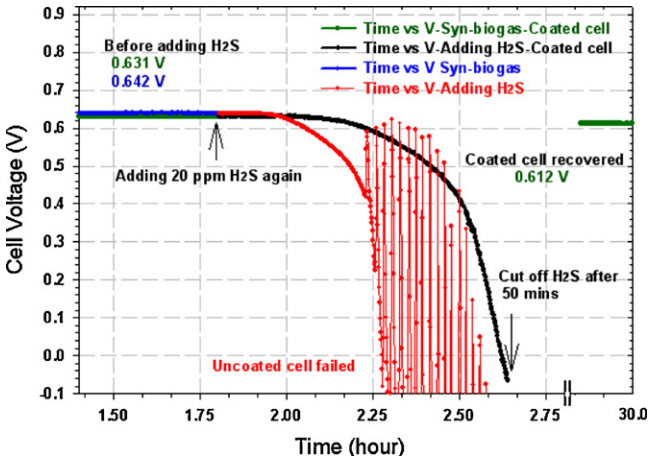

Fig. 14. The impedance spectra of the Ni–CeO_2 coated cell. Before adding 20 ppm H_2S, dotted curve, after the first cycle adding H_2S, triangle curve, and after the second cycle adding H_2S in the diamond curve.

lost just 20 mV (Fig. 14). Moreover, the voltage for the uncoated cell fluctuated widely during the recovery period. The impedance data show that the series resistance slightly increases by 0.02 Ω cm^2 and total polarization resistance changed by 0.10 Ω cm^2 for the coated cell (Fig. 12). After cooling the cell to room temperature and checking the Ni–CeO_2 coated cell, there were no visible carbon deposits on the coated anode surface or in the cell cross-section (Fig. 15). The Ni–CeO_2 coating completely suppressed coke formation and contact cracking, while modestly increasing the tolerance toward H_2S in the biogas.

3.4. SEM micrographs and EDS spectra

SEM images of the cross-section of the uncoated and coated cells after two cycles of exposure to 20 ppm H_2S in IASR are shown in Fig. 16(a) and (b). The poisoned uncoated anode cross-section shows that the surface of the nickel particles became much rougher than that of the coated cell. The nickel particles were reconstructed during exposure to syn-biogas with the H_2S contamination. The image Fig. 16(b) provides evidence that the Ni–CeO_2 coated cell microstructure is still in good shape after H_2S attack. The EDS spec-

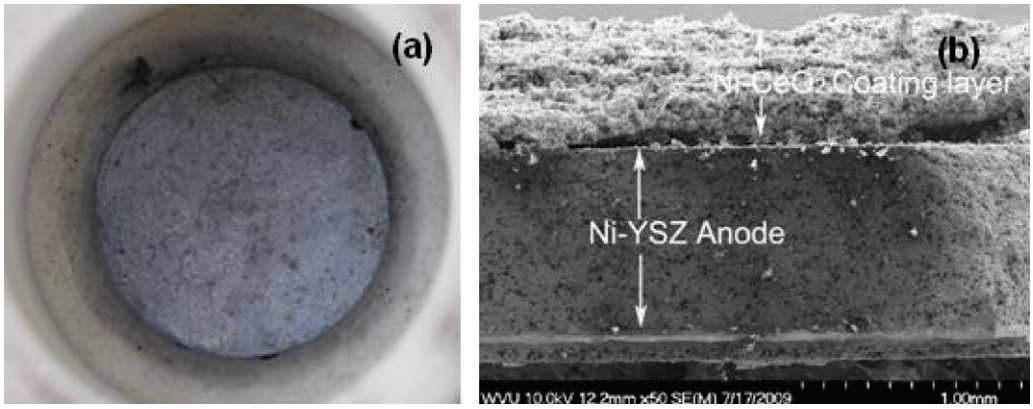

Fig. 15. (a) The Ni–CeO_2 coated cell anode image after recovery from two H_2S contamination cycles. There is no coking on the cell anode. (b) The cell cross-section image. The exposed cell region is about 2 cm diameter.

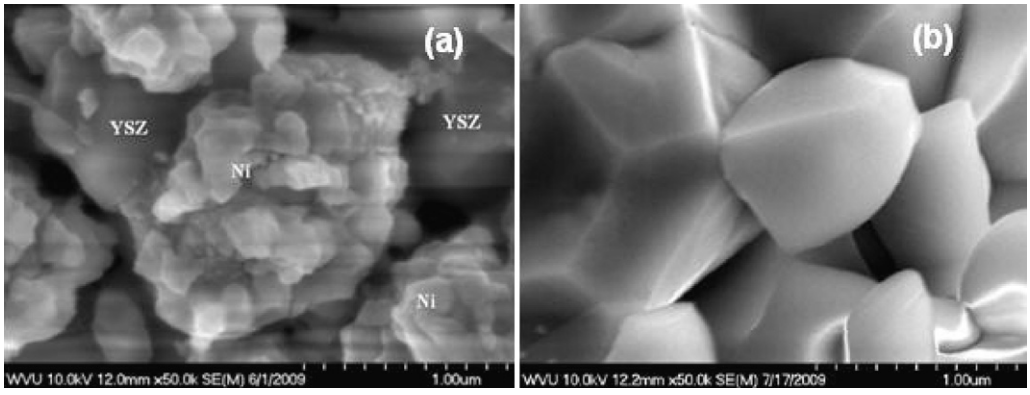

Fig. 16. The 50 K magnification SEM images following two cycles for the H_2S poisoned uncoated cell anode cross-section (a) compared to that of the coated cell anode cross-section (b).

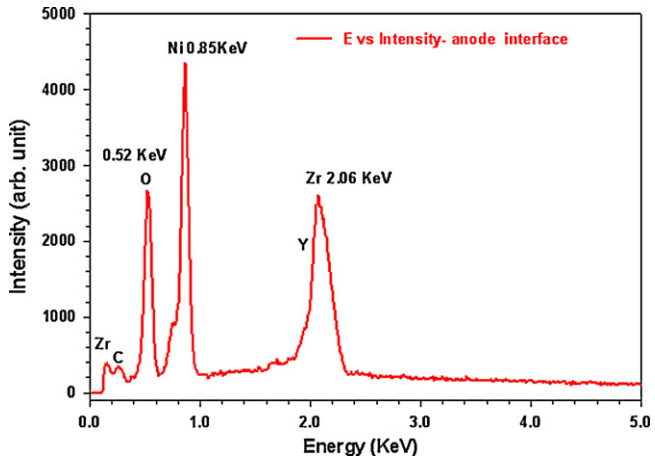

Fig. 17. The EDS spectrum of the uncoated cell anode interface shows the high oxygen peak after H_2S attacking in IASR.

trum of near the anode–electrolyte interface of the uncoated cell in Fig. 17 shows the Ni–YSZ peaks. The high oxygen peak implies that the rough nickel particles after H_2S attack in the case of IASR are nickel oxide. The carbon signal is not significant which indicates that the IASR in these experiments does not result in much coking at the Ni–YSZ anode–electrolyte interface. There are no detectable signals from sulfur in the EDS spectrum. These data clearly show that nickel was oxidized during the Ni–YSZ anode exposure to syn-biogas with 20 ppm H_2S impurity. The cell electrolyte detaching from the anode resulted in nickel oxidation as oxygen was able to reach the anode directly. The SEM images provide evidence that the Ni–CeO_2 coated cell can increase the cell's tolerance toward the H_2S contaminant.

3.5. XRD and XPS spectra

The evidence for significant coking on the cell anode by the IDR case is provided by the XRD spectra in line "a" of Fig. 18. The peak positions of YSZ, Ni, NiO and carbon are listed in Table 1 by 2θ locations [23–26]. The carbon (graphite) peak at 26.26° indicates that the carbon deposited on the cell anode significantly in the IDR case. The spectra of the anode open surface for the ISR and IASR cases after adding H_2S do not show any carbon (graphite) signal. For the ISR case, the NiO peak intensity at 36.90°, 43.07° and 62.61° is stronger at the anode–electrolyte interface than that at the anode open surface in Fig. 18(b) and (c). This implies that the concentration of NiO at the anode–electrolyte interface is higher than that on the anode surface. For the IASR case, the oxygen partial pressure on the cell anode would be much higher than for the ISR case. Both the cell anode surface and the interface show strong NiO peaks in Fig. 18(d) and (e). The spectrum of the Ni–CeO_2 coating surface for the IASR case displays both Ni and CeO_2 signals in Fig. 18(f). The coated cell of for the ISR case had a similar XRD spectrum but showed stronger CeO_2 signals [27] due to the thicker Ni–CeO_2 coating for IASR case. There is no detectable sulfur signal appearing in any of the XRD spectra.

Table 1
XRD peak list 2θ°.

YSZ [23]	Ni [24]	NiO [25]	Carbon [26]	CeO_2 [27]
29.82°	44.17°	36.90°	26.26°	28.60°
34.62°	51.52°	43.07°	44.36°	33.20°
49.91°		62.61°		47.73°
59.39°				56.65°
62.31°				59.48°
				69.50°

To detect any sulfur trace species, XPS was employed for surface chemical analysis. The XPS spectra of the H_2S poisoned uncoated cell for the IASR case basically display the typical C, O, Ni, Y, Zr and NiO signals. In the detailed spectrum in Fig. 19, the S_{2p} is observed on both the interface and surface of the uncoated cell anode at 164.80 eV which is a neutral sulfur phase (Fig. 19(a) and (b)), suggesting that sulfur adsorbs on the Ni–YSZ anode. For the H_2S poisoned coated cell in the IASR case, there is no significant S_{2p} peak on the cell anode interface and on the Ni–CeO_2 coating layer in Fig. 19(c) and (d). This finding supports the fact that the Ni–CeO_2 layer can be a barrier to moderate sulfur adsorption onto the cell anode. Comparing the two peaks of Y_{3d} at 157.50 eV and 159.40 eV, the S_{2p} signal is relatively weak. Moreover, the sulfur trace was not detected by EDS or XRD, the sulfur only resides on the very surface level of the nickel particles.

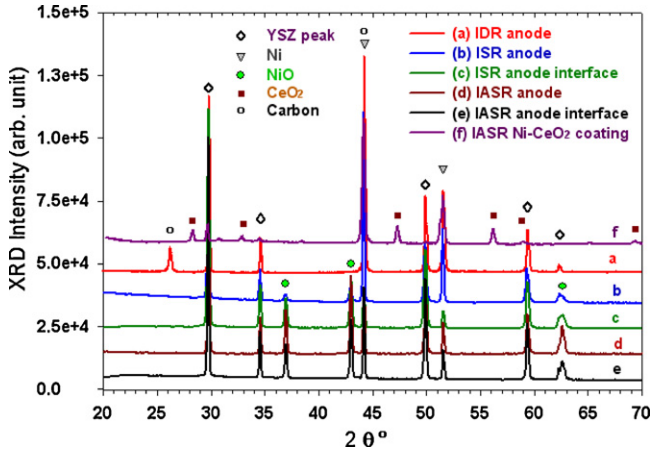

Fig. 18. XRD spectra of the postmortem cell anode: (a) IDR syn-biogas. (b) ISR syn-biogas and poisoned by 20 ppm H_2S, and (c) the cell anode interface. (d) IASR syn-biogas and poisoned by 20 ppm H_2S, (e) the cell anode interface and (f) Ni–CeO_2 coating layer.

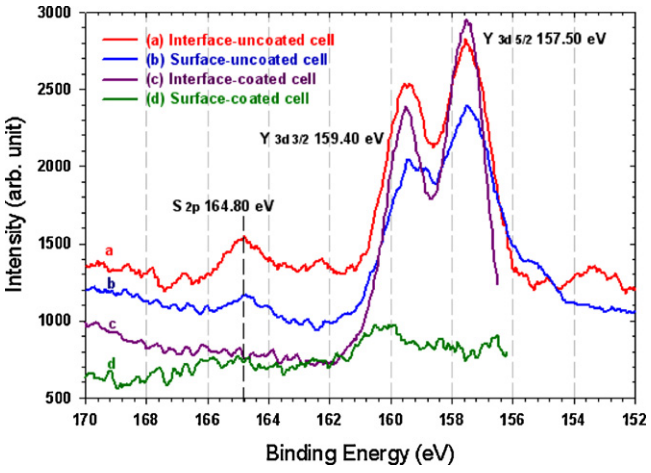

Fig. 19. The XPS spectra of the H_2S poisoned postmortem cell of IASR case. A small S_{2p} peak is observed at 164.80 eV in both spectra (a) interface and (b) surface of uncoated cell. The S_{2p} peak is insignificant in the spectrum of the coated cell interface (c) and on the Ni–CeO_2 coating layer (d). Y_{3d} has two main peaks at 157.50 eV and 159.40 eV on the Ni–YSZ anode spectra (a), (b) and (c).

4. Discussion

4.1. Electrochemical and thermodynamic analysis for the uncoated SOFC

The best cell performance in the IDR case was given at the reforming temperature of 850 °C. The impedance spectra in Fig. 4 show that the polarization resistance increased by only 0.026 Ω cm^2 during the test, which will cause an increase of overpotential of 13 mV. This is in good agreement with the data for the cell degradation of about 1.5% as measured from the cell voltage loss during 110 h in Fig. 3(a). However, the cell was severely coked and the current collection meshes partially lost contact with the anode surface. The damage of the contacts during reforming results in an increased series resistance of about 0.033 Ω cm^2. The coke layer on the Ni–YSZ anode surface could eventually obstruct the fuel reaching the cell interface and reduce the CH_4 reforming rate. The examination of the postmortem cell shows that the carbon tends to be deposited only on the anode surface. This observation suggests that a "carbon resistive" reforming catalysts could be used on the top surface of Ni–YSZ anode to prevent coking. The deposited carbon on the cell surface is porous and electrically conductive. The cell contact cracking and coking did not lead to severe loss of cell performance. The damaged contacts on the anode surface may be caused by the endothermic reactions during the CH_4 reforming:

$$CH_4 \rightarrow C + 2H_2 \qquad \Delta H^{\circ}_{298\,K} \sim 75.9\ \text{kJ mol}^{-1} \tag{1}$$

$$CH_4 + CO_2 \rightarrow 2CO + 2H_2 \qquad \Delta H^{\circ}_{298\,K} \sim 247.1\ \text{kJ mol}^{-1} \tag{2}$$

where H°_{298} is the standard enthalpy of reaction at 298 K. The endothermic reactions (1) and (2) can lead to local area cooling such that the unmatched thermal expansion between the anode and the contacts could cause separation of the contact from the cell anode. Reaction (1) also causes carbon deposition by methane pyrolysis. A high current loading to the cell can partially compensate for the heat lost from the endothermic reaction and can help to reduce coking [3]. The 0.5 A cm^{-2} current density load here obviously was not high enough to overcome the coking and cracking.

From theoretical equilibrium calculations (TEC) for the clean biogas (only CH_4 and CO_2), the best reforming product combination of H_2 and CO occurs with the ratio of CH_4 to CO_2 close to one at 850 °C (Fig. 20). The higher reforming temperature gives a higher H_2 mole concentration in the product gas (Fig. 21). The maximum reforming temperature 850 °C which provides over 96% CH_4 reforming conversion efficiency was utilized in the long-term testing to avoid breaking the silver current collection wire. TEC predict the product concentrations as H_2 47.8%, CO 49.3%, CO_2 0.7%, H_2O 0.8% and CH_4 1.4% with the input biogas near $CH_4/CO_2 = 1$, which should yield the highest IDR reforming efficiency at 850 °C. Thus

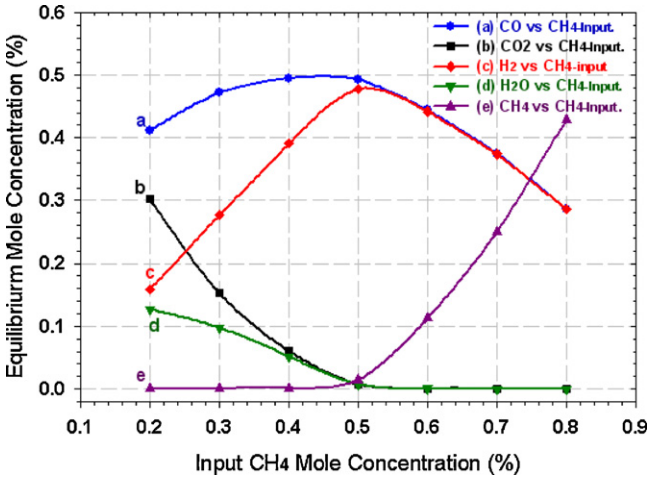

Fig. 20. Thermodynamic calculation of equilibrium concentrations of H_2, CO, CO_2 and H_2O for IDR with input syn-biogas $CH_4/CO_2 = X/1 - X$ at 850 °C. The reforming products mole concentrations are H_2 = 47.8% and CO = 49.3%, at $CH_4/CO_2 = 1$ with the highest H_2 and CO conversion efficiency.

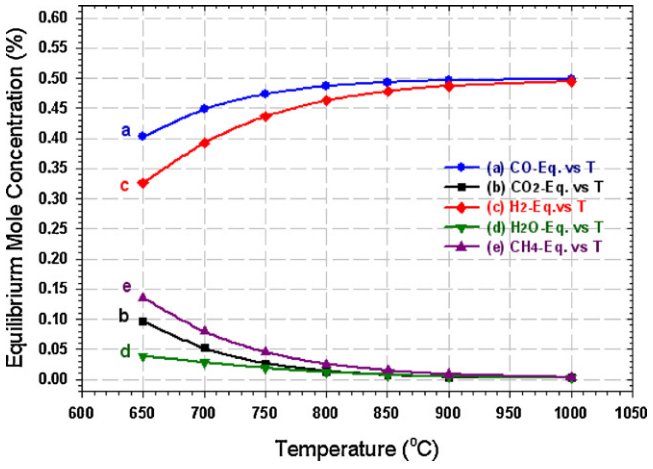

Fig. 21. The equilibrium mole concentrations of H_2, CO, CO_2 and H_2O change as a function of the reforming temperature with the input clean biogas $CH_4/CO_2 = 1$.

the $CH_4/CO_2 = 1$ is used in the IDR cases. TEC also predict that solid carbon (graphite) could be produced for IDR reforming. The experimental OCVs at 750 °C, 800 °C and 850 °C are about 80–100 mV lower than those of the theoretical OCVs which are calculated by the Nernst equation for IDR under thermodynamic equilibrium with $CH_4/CO_2 = 1$ in gas phase in Table 2. But the experimental

Table 2
Biogas reforming summary table.

Reforming condition	OCV[a] experimental	OCV theoretical	Cell voltage 0.5 A cm^{-2}	Contact cracking, coking	Voltage loss before H_2S	Recovery H_2S
IDR at 750 °C	0.994 V	1.055 V	0.552 V for 2 h			
IDR at 800 °C	1.025 V	1.072 V	0.631 V for 2 h			
IDR at 850 °C	1.049 V	1.092 V	0.720 V for 110 h	Yes, Yes[b]	10 mV	0.650 V[c]
ISR at 850 °C	0.925 V	0.985 V	0.647 V for 115 h	Yes, Yes	No	
ISR at 850 °C	0.967 V	0.985 V	0.732 V for 306 h	No, No	No	0.642 V[c]
Coated cell						0.631 V[c]
IASR at 850 °C	0.962 V	0.998 V	0.647 V for 74 h	Slight, a few	No	0.612 V[d]
IASR at 850 °C	0.953 V	0.998 V	0.660 V for 70 h	No, No	No	
Coated cell						
H_2 + 3% H_2O at 800 °C	1.072 V	1.110 V	0.785 V for 2 h	No, No	No	

[a] The OCV is measured under fuel flow of about 200 sccm.
[b] Theoretical calculation predicted coking.
[c] The first cycle adding H_2S.
[d] The second cycle adding H_2S.

OCV showed the same trend as did the theoretical OCV with temperature. The low experimental OCV indicates that the predicted theoretical OCV from ideal thermodynamic equilibrium was not achieved due to solid carbon pollution and the non-static, flowing fuel system. The theoretical OCV most likely overestimates the partial pressures of H_2 and CO. Gas leakage could be another reason for the experimental OCV drop of 30–40 mV. The low experimental OCV was also observed in the ISR and IASR cases as well.

For the ISR case, the cell performance did not show any degradation (Fig. 3(b)) before adding H_2S. The impedance spectra indicated that the polarization resistance remained almost constant (Fig. 6). The theoretical thermodynamic equilibrium calculation predicts that the reformed products at 850 °C are 53% H_2, 15.3% H_2O, 25% CO, 6.7% CO_2 and CH_4 less than 0.05% from the input fuel composition of 32% CH_4, 48% H_2O, and 20% CO_2. The cell experimental OCV is 0.925 V which is unusually lower than the theoretical OCV of 0.985 V (Table 2). It implies that the biogas reforming did not reach equilibrium. The coking on the surface of the postmortem cell was significantly reduced in this case, because the steam reforming reaction (3) can reduce the rate of coke formation from reaction (1):

$$CH_4 + H_2O \rightarrow CO + 3H_2 \qquad \Delta H^{\circ}_{298\,K} \sim 205.9\ \text{kJ mol}^{-1} \tag{3}$$

However, the current collection contacts were still cracked in the ISR case which could explain the increase of the cell series resistance (Fig. 6). This could result from the non-uniform thermal expansion caused by the endothermic reactions (1)–(3). When the cell is under a certain current loading, joule heating can compensate for a portion of the heat needed for the endothermic reactions and the thermal expansion effect may be mitigated. But the 0.5 A cm^{-2} load here is not enough to prevent the damage to the contacts. As an alternative way to prevent the cracking current collector during reforming, IASR was introduced. The partial oxidation reforming and combustion reactions are

$$CH_4 + 0.5O_2 \rightarrow CO + 2H_2 \qquad \Delta H^{\circ}_{298\,K} \sim -35.9\ \text{kJ mol}^{-1} \tag{4}$$

$$CH_4 + 2O_2 \rightarrow CO_2 + 2H_2O \qquad \Delta H^{\circ}_{298\,K} \sim -802.6\ \text{kJ mol}^{-1} \tag{5}$$

The partial oxidation reaction (4) is exothermic and could compensate for the heat needed in the endothermic reactions (1)–(3). The thermodynamic equilibrium calculation shows that the CH_4/O_2 ratio of 2 gives the maximum H_2 production from reaction (4) [28]. A higher CH_4/O_2 ratio will result in significant combustion of CH_4 by reaction (5). For the uncoated cell, the IASR results indicate the heat balance was not fully achieved and the cell contacts still exhibited tiny cracks. But IASR nearly eliminated the carbon deposition on the anode surface and also prevented the contact cracking for the coated cell. In this case the exothermic reactions (4) and (5) produced enough heat to prevent contact cracking. This extra heat was indicated by an increase in the cell temperature of 3–847 °C as compared to the ISR case. The theoretical thermodynamic equilibrium calculation indicates that over 99.95% CH_4 is converted to H_2 and CO at 850 °C for the IASR. The composition of the reformed products is 42.7% H_2, 9.3% H_2O, 27.1% CO, 5.4% CO_2, and 15.4% N_2. The cell experimental OCV is 0.962 V which is close to the theoretical OCV of 0.998 V (Table 2) after taking into account about 30 mV loss by fuel leaking. Because of the 350 μm Ni–CeO_2 coating layer on the coated cell, the experimental OCV of the coated cell is 9 mV lower than that of the uncoated cell. From the OCV performance data in the IASR case, the fuel utilization efficiency is better than the IDR and ISR cases.

When 20 ppm H_2S was added to the syn-biogas fuel, the cell quickly degraded for the uncoated cell in both the ISR and IASR cases. The cell electrolyte was cracked after exposure to syn-biogas with 20 ppm H_2S in a few hours, a phenomenon never seen in the previous tests with 20 ppm H_2S in H_2 or syngas fuel (Fig. 7). This suggests that the poisoning effect of H_2S in syn-biogas fuel is much more severe and rapid than that using hydrogen or coal syngas as the fuel. These different degradation behaviors imply that after adding H_2S, the CH_4 in the fuel did not reform efficiently to produce H_2 and CO, and the partial pressure of oxygen could be high enough to form NiO at anode/electrolyte interface. The Ni catalyst in the cell anode plays roles of both reforming CH_4 and triggering H_2 to generate water in the electrochemical reaction. If Ni loses its function as a catalyst by adsorbing sulfur or forming nickel sulfur compounds, the reforming rate could be significantly reduced so that the triple phase boundary (TPB) of the cell anode would functionally fail in the existing environment. The subsequent Ni oxidation reaction caused a volume expansion in the Ni–YSZ cermet so that the electrolyte completely separated from the anode.

4.2. Ni–CeO_2 coated SOFC electrochemical and thermodynamic analysis

For the ISR case, the Ni–CeO_2 coated cell showed stable series and polarization resistances in the impedance spectra (Fig. 8) for the 304 h before adding 20 ppm H_2S. The Ni–CeO_2 barrier played roles of both CH_4 reforming and H_2S adsorption. Ni doped ceria is one of the most active catalysts for the water-gas-shift reaction [29].

$$CO + 2CeO_2 \rightarrow CO_2 + Ce_2O_3 \tag{6}$$

$$H_2O + Ce_2O_3 \rightarrow 2CeO_2 + H_2 \tag{7}$$

The desired reactions (2)–(4) of CH_4 internal reforming were more favorable when the product CO was consumed by reaction (6). In this case, the rate of reaction (1) could be reduced relatively so that the coking was restrained. These statements are supported by the consistent performance and stable series resistance of the Ni–CeO_2 coated cell in 304 h test before adding 20 ppm H_2S (Figs. 8 and 9). After adding 20 ppm H_2S, the Ni–CeO_2 coated cell still degraded in 4 h. However, and more importantly, the cell did not crack and could be recovered to over 95% of its former performance. For the ISR case, the Ni–CeO_2 coating was about 100 μm thick. The cell contacts still had minor cracks after running about 324 h. The heat required by the endothermic reactions had not been completely compensated for by the exothermic reaction. Moreover, the thickness of the coating may be too thin to relieve the thermal strain. In the IASR case, the cell anode was coated with about a 350-μm layer of the Ni–CeO_2. The contact cracking was completely eliminated with the partial oxidation reactions (4) and (5). Both these Ni–CeO_2 coated cells have shown a modest increase of tolerance for H_2S attack. In previous work, CeO_2 was used as a desulfurization sorbent to remove H_2S, because CeO_2 is a regenerable catalyst at high temperature (over 600 °C) in a reducing environment [30]:

$$CeO_2(s) + (2-n)H_2(g) \rightarrow CeO_n(s) + (2-n)H_2O(g) \tag{8}$$

$$2CeO_n(s) + H_2S(g) + (2n-3)H_2(g) \rightarrow Ce_2O_2S(s) + 2(n-1)H_2O(g) \tag{9}$$

where $1.5 < n < 2.0$ for example. Zeng et al. reported that the H_2S concentration was reduced from 10,000 ppm to less than 10 ppm in the product gas at 850 °C using a ceria sorbent. The Ni–CeO_2 coating layer over the Ni–YSZ anode and the mesh contacts is easy to implement compared to ceria doping or impregnation in the Ni–YSZ anode. The Ni–CeO_2 coating helps to maintain the excellent electrical conductivity, electrochemical properties and high temperature stability of the Ni–YSZ anode. In the ISR and IASR cases, the barrier Ni–CeO_2 layer contains 90% Ni for reforming CH_4 and exciting reactions (6) and (8). The 10% CeO_2 aids in desulfurization by

reaction (9) in which Ni–CeO_2 has displayed some desulfurization ability, but not as good as anticipated. To achieve high efficiency of desulfurization by CeO_2, the CeO_2 must be pre-reduced to CeO_n in a reducing environment. If the O_2 partial pressure is over 10^{-16} atm, CeO_2 will largely lose the function of desulfurization [31]. Besides the desulfurization function of ceria, the nickel amount (90%) in Ni–CeO_2 coating layer can slightly postpone the cell degradation time by a process of sulfur adsorption. The H_2S tolerance of Ni–CeO_2 is thus a co-effect of the both ceria and nickel. The Ni/Ce combination used here may not be the most efficient one and will need to be optimized. A higher CeO_2 sorbent concentration along with the addition of ZrO to CeO_2 may improve the cell's tolerance to H_2S when using biogas with 20 ppm H_2S. More experimental work is required in this area.

5. Conclusion

The internal dry (IDR), steam (ISR) and air with steam (IASR) reforming of clean biogas on an anode-supported SOFC have been evaluated. The basic barriers of implementing internal reforming of clean biogas are coking and differential thermal expansion by the endothermic reforming reactions on the cell anode. The steam present in the reforming reactions (ISR) can largely reduce coking. The endothermic reforming reactions can cause severe cracks in the cell contacts and the cell anode. Introduction of the partial oxidation reforming reaction can moderate the thermal effects from the endothermic reactions and minimize coking on the anode surface. The IASR case is one example of achieving the internal reforming of clean biogas on a SOFC The Ni–CeO_2 coating layer can improve biogas reforming without cracking and coking at 850 °C. The application of 20 ppm H_2S to the uncoated cell caused complete cell failure in very short time. When 20 ppm H_2S is injected to the coated cell, the reduction of the biogas reforming on the Ni–YSZ anode is temporarily halted but eventually this cell fails as well. However, nearly complete recovery of cell performance was noted after the H_2S was removed. The H_2S poisoning effects on the Ni–YSZ anode-supported SOFC are much more severe when using biogas fuel than for either H_2 or syngas fuel. The Ni–CeO_2 coating barrier can increase H_2S tolerance somewhat with lower degradation rate and high recoverability. Thus the application of Ni–CeO_2 coating presents a way to suppress coking and cracking while enhancing the resistance to sulfur attack for the Ni based anode.

Acknowledgements

This work is conducted under US DOE (Department of Energy) EPSCoR Program. It is jointly sponsored by US DOE Office of Basic Energy Sciences, NETL (National Energy Technology Laboratory), WV State EPSCoR Office and the West Virginia University under grant number DE-FG02-06ER46299. Dr. T. Fitzsimmons is the DOE Technical Monitor. Dr. R. Bajura is the Administrative Manager and Dr. I. Celik is the Technical Manager and Principal Investigator of this project. Dr. Andy Woodworth, Mr. Liviu Magean, Mrs. Andrienne McGraw are thanked for their help in acquiring the SEM and EDS data.

References

[1] J.V. Herle, Y. Membrezb, O. Bucheli, Journal of Power Sources 127 (2004) 300–312.
[2] A.L. Dicks, Journal of Power Sources 61 (1996) 113–124.
[3] Y. Lin, Z. Zhan, J. Liu, S.A. Barnett, Solid State Ionics 176 (2005) 1827–1835.
[4] R.M. Ormerod, Proceedings of the International Symposium, vol. 122, Brugge, Belgium, April 1999, pp. 35–46.
[5] C.M. Finnerty, R.M. Ormerod, Solid Oxide Fuel Cell VI. The Electrochemical Society Proceedings, Pennington, NJ, 1999, PV, PV 99-19, p. 583.
[6] T. Takeguchi, R. Kikuchi, T. Yano, K. Eguchi, K. Murata, Catalysis Today 84 (2003) 217–222.
[7] S.C. Singhal, K. Kendall, ISSN 14710846 High Temperature Solid Oxide Fuel Cells Fundamentals Design and Applications, Elsevier Ltd., 2005, p. 349.
[8] B. Tu, Y. Dong, B. Liu, M. Cheng, Journal of Power Sources 165 (2007) 120–124.
[9] J. Zhu, D.K. Zhang, K.D. King, Fuel 80 (2001) 899–905.
[10] V. Antonucci, P.L. Antonucci, A.S. Arico, N. Giordan, Journal of Power Sources 62 (1996) 95–99.
[11] M. Gong, X. Liu, J. Trembly, C. Johnson, Journal of Power Sources 168 (2007) 289–298.
[12] J. Dong, Z. Cheng, S. Zha, M. Liu, Journal of Power Sources Short Communication 156 (2006) 461–465.
[13] A. Norheim, I. Waernhus, M. Brostrom, J.E. Hustad, A. Vik, Energy & Fuels 21 (2007) 1098–1101.
[14] E. Perry Murray, T. Tsai, S.A. Barnett, Nature 400 (1999) 649–651.
[15] M. Mogensen, B. Kindl, B. Malmgreen-Hansen, Program and Abstracts of 1990 Fuel Cell Seminar Courtesy Associates, Washington, DC, 1990, p. 195.
[16] M. Mogensen, N.M. Sammes, G.A. Tompsett, Solid State Ionics 129 (2000) 63–94.
[17] O.A. Marina, C. Bagger, S. Primdahl, M. Mogensen, Solid State Ionics 123 (1999) 199.
[18] T. Takeguchi, Y. Kani, T. Yano, R. Kikuchi, K. Eguchi, K. Tsujimoto, Y. Uchida, A. Ueno, K. Omoshiki, M. Aizawa, Journal of Power Sources 112 (2002) 588–595.
[19] Y. Lin, Z. Zhan, S.A. Barnett, Journal of Power Sources 158 (2006) 1313–1316.
[20] H. Devianto, S.P. Yoon, S.W. Nam, J. Han, T. Lim, Short communication, Journal of Power Sources 159 (2006) 1147–1152.
[21] M. Flytzani-Stephanopoulos, M. Sakbodin, Z. Wang, Science 312 (2006) 1508–1510.
[22] C. Xu, J.W. Zondlo, H.O. Finklea, O. Demircan, M. Gong, X. Liu, Journal of Power Sources 193 (2009) 739–746.
[23] H. Horiuchi, A.J. Schultz, P.C. Leung, W. Leung, J.M. Williams, Acta Crystallographica, Section B: Structural Science 40 (1984) 367–372.
[24] M. Yousuf, CH.P. Sahu, H.K. Jajoo, S. Rajagopalan, K. Govinda Rajan, Journal of Physics F 16F (1986) 373–378.
[25] D. Taylor, Transactions and Journal of the British Ceramic Society 83 (1984) 5.
[26] O. Hassel, H. Mark, Zeitschrift Fur Physik 25 (1924) 317.
[27] J.D. Hanawalt, H.W. Rinn, L.K. Freverl, Analytical Chemistry 10 (1938) 475.
[28] J. Zhu, D. Zhang, K.D. King, Fuel 80 (2001) 899–905.
[29] S. Hilaire, X. Wang, T. Luo, R.J. Gorte, J. Wagner, Applied Catalysis A: General 258 (2004) 271–276.
[30] Y. Zeng, S. Kaytakoglu, D.P. Harrison, Chemical Engineering Science 55 (2000) 4893–4900.
[31] H. He, R.J. Gorte, J.M. Vohs, Electrochemical and Solid-State Letters 8 (6) (2005) A279–A280.